

Doctoral Thesis

Optical Follow-Up of High-Energy Neutrinos

Simeon Reusch

March 21, 2023

Humboldt-Universität zu Berlin

Copyright

©@ This book is released into the public domain using the CC0 code. To the extent possible under law, I waive all copyright and related or neighbouring rights to this work. To view a copy of the CC0 code, visit: <http://creativecommons.org/publicdomain/zero/1.0>

This thesis was typeset with the help of KOMA-Script and L^AT_EX using the kaobook class.

The code used to typeset this thesis and create the figures within can be accessed at github.com/simeonreusch/thesis

Publisher

First published in August 2023 by Humboldt-Universität zu Berlin

Contents

Contents	iii
1 The IceCube Detector	1
1.1 Cherenkov radiation	1
1.2 IceCube instrumentation	2
APPENDIX	5
Bibliography	7

List of Figures

1.1	Cherenkov radiation	1
1.2	Cherenkov spectrum	2
1.3	PMT schematic	2
1.4	IceCube digital optical module	3
1.5	IceCube DOM connections	3
1.6	IceCube side-on	4
1.7	IceCube top-down view	4
1.8	IceCube drill	4

List of Tables



1 The IceCube Detector

One of the two most relevant instruments for this thesis is the *IceCube Detector*, a neutrino detector located at the geographic South Pole. It is the successor to the Antarctic Muon And Neutrino Detector Array (AMANDA) at the same location [1, 2].

The basic operational principle of IceCube (and already of AMANDA) is the detection of Cherenkov light within the antarctic ice. When charged secondary particles created by neutrino interactions travel through the ice, their speed exceeds the phase velocity of light in ice and they emit Cherenkov radiation. The detector consists of 5160 individual digital optical modules (DOMs), buried deep in the ice. These are sensitive to the Cherenkov radiation.

1.1 Cherenkov radiation

Cherenkov radiation was first detected in 1934 by Soviet scientist Pavel Cherenkov [4]. It occurs when charged particles travel within a medium with a velocity exceeding the speed of light in that medium. The refractive index in a medium is defined as $n = \frac{c_0}{c_m}$, where c_m is the speed of light in vacuum and c_m is the phase velocity of light in that medium. Note that the phase velocity of light in a medium can exceed c_0 , so $n < 1$ is possible.

When charged particles cross an electrically neutral dielectric medium, atoms along the particle's path are briefly polarized and emit electromagnetic radiation.

For slow particles, this radiation destructively interferes with itself, canceling out all signals (see the bottom panel of Fig. 1.1). Now, if the particle is travelling faster than speed of light within the medium c_m , this destructive interference does not happen. Rather, a cone-shaped wavefront gets created (see top panel of Fig. 1.1). This wavefront constitutes Cherenkov radiation. If the particle has speed $v = \beta c_0$, the angle θ between the particle trajectory and the direction of the Cherenkov radiation can be calculated as [3]:

[1]: Andrés et al. (1999), *The AMANDA neutrino telescope*

[2]: Andrés et al. (2000), *The AMANDA neutrino telescope: principle of operation and first results*

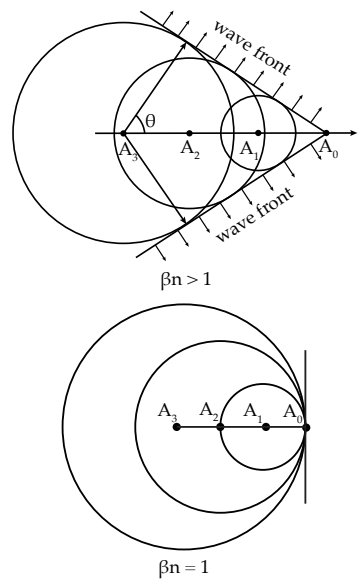


Figure 1.1: The principle of Cherenkov radiation. In the upper figure Cherenkov radiation is emitted, as the radiation emitted at different points in time forms mutual wavefronts. In the figure on the bottom, all radiation is cancelled out by destructive interference (all circles are subsets of the first on the left, as the particle is not moving faster than light in the medium). Adopted from [3].

[4]: Cherenkov (1934), *Visible emission of clean liquids by action of gamma radiation*

[3]: L'Annunziata (2020), *Handbook of Radioactivity Analysis. Volume 1: Radiation Physics and Detectors*

$$\cos \theta = \frac{\beta}{n} \quad (1.1)$$

1: This is of course rather crude. The n of Antarctic glacial ice depends e.g. on depth; a fact we will come back to later when discussing directional reconstruction of high-energy IceCube neutrinos.

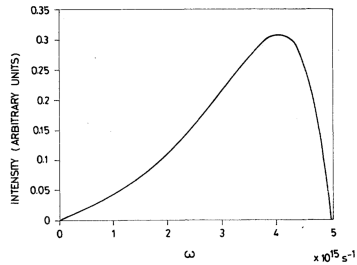


Figure 1.2: Cherenkov spectrum for a particle with $v = 0.8 c_0$ in water. The intensity peaks at $4 \times 10^{15} \text{ Hz}$, corresponding to a wavelength of 75 nm, lying at the high-frequency end of the UV spectrum. From [5].

[5]: Filöp et al. (1992), *Cherenkov radiation spectrum*

[6]: Iams et al. (1935), *The Secondary Emission Phototube*

For example: If the medium is ice, to first order the refractive index $n \approx 1.31$.¹ A secondary muon traveling through the ice at $0.999 c_0$ will therefore emit Cherenkov light at an angle of $\theta = \cos^{-1} \left(\frac{0.999}{1.31} \right) \approx 40^\circ$.

Cherenkov radiation does not have spectral peaks, but is continuous, with a relative intensity proportional to the frequency. Note that the refractive index of a medium is also frequency dependent, dropping below 1 in the X-ray. From this it follows that Cherenkov radiation appears blue to the human eye (the high-frequency part dominates) and peaks in the ultra violet (UV), before it sharply drops off in the X-ray regime [5], see Fig. 1.2.

1.2 IceCube instrumentation

IceCube detects neutrinos by observing the optical part of their secondary particle Cherenkov spectrum (see section 1.1 above). To understand how this is done, one first needs to look at the working principle of a photomultiplier tube (PMT).

Photomultiplier tubes

A PMT is a device used to detect very faint light signals by amplifying them. They consist of vacuum tubes and were successfully realized for the first time in the 1930s [6].

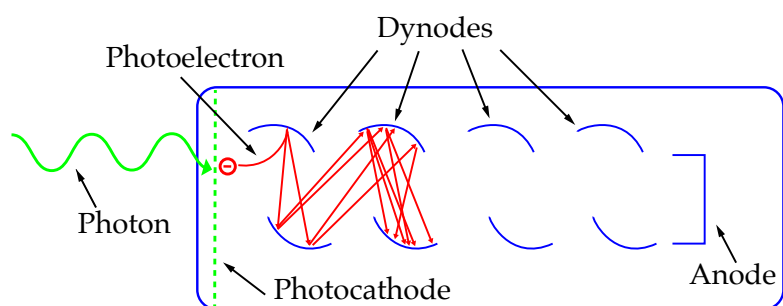


Figure 1.3: A photomultiplier tube. Adopted from [7].

[8]: Einstein (1905), *Über einen die Erzeugung und Verwandlung des Lichtes betreffenden heuristischen Gesichtspunkt*

As one can see in Fig. 1.3, there are three principal components: a *cathode*, a number of *dynodes* and an *anode*. When photons hit the cathode, they can release electrons via the photoelectric effect [8]. These photoelectrons are then accelerated (towards the right side in Fig. 1.3) by an electric field within the tube. This field is generated by applying a high voltage between the cathode and the anode.

To amplify the signal, a number of dynodes is placed in between. These are additional electrodes with subsequently higher voltages. When the photoelectron hits the first dynode, a number of secondary electrons are generated, which are then accelerated towards the next dynode by the electric field. This process repeats for every dynode, generating an avalanche of electrons exponentially amplifying the original single

photoelectron signal. The number of secondary electrons hitting the anode is proportional to the number of incident photons, resulting in a linear detector response (as long as the detector stays below its saturation level) [9].

IceCube uses PMTs made by Hamamatsu Photonics (R7081-02), sensitive to photons between 300 nm and 650 nm. They have a quantum efficiency at 390 nm of 25%, are operated with a voltage of 1500 V and have a gain of 10^7 . The photon-sensitive surface area is typically 530 cm^2 [10].

The Digital Optical Module

The individual IceCube PMTs for detecting the Cherenkov radiation are enclosed in *digital optical modules* (DOMs). Each DOM consists of a pressure-resistant glass sphere, several controller boards and the PMT, facing downward (see Fig. 1.4). The glass sphere can withstand long-term pressure of 250 bar. The optical transmission of the spheres was measured to be 93% at 400 nm, decreasing to 10% at 315 nm.

The circular main board hosts data acquisition and control, as well as units for communication, calibration and a power converter. Another board interfaces with the PMT, while additional boards delay the PMT signals, generate the high voltage current powering the PMT, as well as control calibration light emitting diodes (LEDs) that generate light flashes which can be received by neighboring DOMs for calibration purposes [11].

Because of data storage restrictions, the DOMs only record the full digitized waveform data after a “hit”. A hit is triggered when also DOMs above and below the DOM in question (to be precise, the neighbors and the next-to-nearest neighbors) report a coincident signal above a certain threshold [11]. To fully record the waveform after a hit, there needs to be some kind of buffer. This is realized with the delay board, which routes the analog PMT signal through a 10 m long, serpentine copper trace to delay it by 75 nm.

The DOMs are connected to the IceCube Laboratory (ICL) with twisted-pair copper cables. The power for the DOM is also transmitted with this cable. Two DOMs share one twisted-pair cable, and each DOM is also directly connected to its two neighbors on the same string (to detect hits, i.e. locally coincident signals).

The flasher board houses 12 LEDs operating at ~ 400 nm wavelength. These are used to verify the DOM timing response, to measure the DOM in-ice position, to determine the optical properties of the ice, and to verify the reconstruction algorithms [11].

Detector layout and deployment

In total, approximately 5800 DOM units were built and tested, 300 failing tests and the rest being delivered to the South Pole. The vast majority of these were ultimately deployed (5160 in total). The final detector layout (since the last drilling campaign 2010/2011, see below) consists of 86 strings. The DOMs were deployed along those strings, like pearls on a necklace. Each string contains 60 DOMs.

[9]: Wright (2017), *The Photomultiplier Handbook*

[10]: Abbasi et al. (2010), *Calibration and characterization of the IceCube photomultiplier tube*

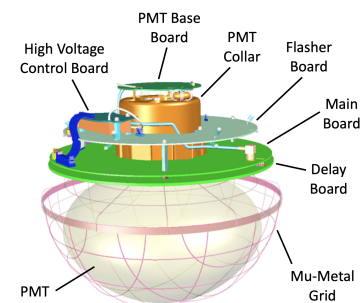


Figure 1.4: The IceCube DOM seen from the side. The detecting side of the PMT is facing downwards, with the main board on the PMT base board on top. From [11].

[11]: Aartsen et al. (2017), *The IceCube Neutrino Observatory: instrumentation and online systems*

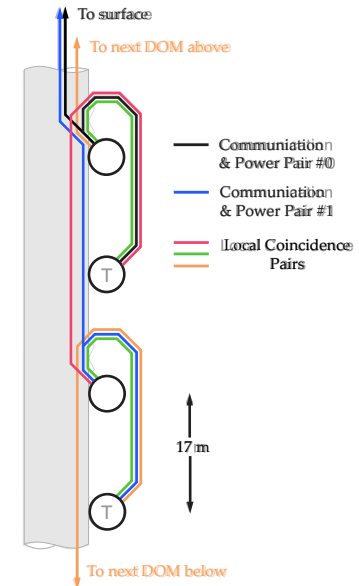


Figure 1.5: Connection scheme for four IceCube DOMs along one string. Pairs of DOMs share one twisted-pair cable. Also, each DOM is directly connected to its direct neighbor above and below. Adopted from [11].

The instrumented part of the chains starts at 1450 m below surface, with one DOM every 17 m to a depth of 2450 m, just above the bedrock at a depth of 2820 m. In Fig. 1.6 the layout of the in-ice array can be seen. The strings follow a roughly hexagonal layout (see Fig. 1.7), with a side length of 1 km². The total instrumented volume of glacial ice is thus 1 km³ [11]. Of the 5160 deployed DOMs, 43 are dead as of March 2023, a loss of less than 1%.

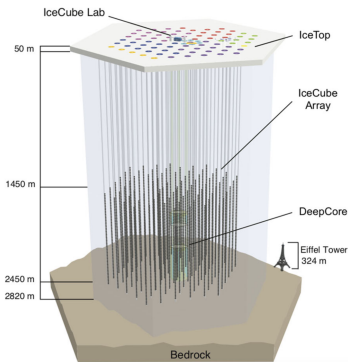


Figure 1.6: Side view of the IceCube detector, showing the instrumented array deep in the antarctic glacial ice. In the center on top is the IceCube Laboratory, were data acquisition takes place. From [12].

As one can imagine, embedding the DOMs within the ice was a non-trivial task. It required drilling 86 boreholes with a diameter of roughly 60 cm and a length of 2500 m. This was achieved over several drilling campaigns with the Enhanced Hot Water Drill (EHWD) specifically built for this task. This drill had a total power of 5 MW and was able to drill with a maximum speed of 2.2 m min⁻¹. With these performance characteristics, one hole could be drilled every 48 h [11]. It took 7 drilling seasons to deploy the final IceCube86 setup, from the Antarctic summers 2004/2005 to 2010/2011. Fig. 1.8 shows the tower operations site directly above the bore hole [13].

The water for drilling the holes was heated with 35 water heaters working in parallel, each providing 125 kW power. The average amount of fuel used per drill hole was 27 000 L [13].

IceTop

One of the major classes of background events are cosmic ray interactions in the atmosphere, as the muons generated in these are indiscernible from neutrino-induced muons within the in-ice array. IceTop serves as a partial veto against these. The detector array consists of 2 × 81 ice-filled Cherenkov tanks. These are placed in pairs on the same hexagonal grid as the DOM strings for the in-ice array. Each tank is equipped with two IceCube DOMs (see The Digital Optical Module above).

Data acquisition

asdf

Figure 1.7: Top-down view of the IceCube detector, spanning 1 km² on the surface. Adopted from [12].

[13]: Benson et al. (2014), *IceCube Enhanced Hot Water Drill functional description*

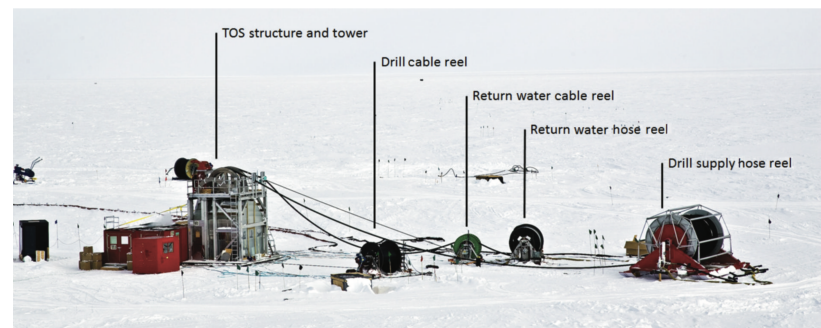


Figure 1.8: The hole drilling part of the IceCube Enhanced Hot Water Drill, excluding the hot, pressurized water supply. One can see the tower operations site (TOS) above the hole and the hoses providing hot water and returning cooled water from the bore hole to the generators in a closed loop. From [13].

APPENDIX

Bibliography

- [1] AMANDA Collaboration, E. Andrés et al. "The AMANDA neutrino telescope". In: *Nuclear Physics B - Proceedings Supplements* 77.1-3 (1999), pp. 474–485. doi: [10.1016/s0920-5632\(99\)00469-7](https://doi.org/10.1016/s0920-5632(99)00469-7) (cited on page 1).
- [2] AMANDA Collaboration, E. Andrés et al. "The AMANDA neutrino telescope: principle of operation and first results". In: *Astroparticle Physics* 13.1 (2000), pp. 1–20. doi: [10.1016/s0927-6505\(99\)00092-4](https://doi.org/10.1016/s0927-6505(99)00092-4) (cited on page 1).
- [3] M. F. L'Annunziata. *Handbook of Radioactivity Analysis. Volume 1: Radiation Physics and Detectors. Radiation Physics and Detectors.* 4th ed. Elsevier Science & Technology Books, 2020 (cited on page 1).
- [4] P. A. Cherenkov. "Visible emission of clean liquids by action of gamma radiation". In: *Doklady Akademii Nauk SSSR* 8 (1934), pp. 451–454 (cited on page 1).
- [5] L. Filöp and T. Biró. "Cherenkov radiation spectrum". In: *International Journal of Theoretical Physics* 31.1 (1992), pp. 61–74. doi: [10.1007/bf00674341](https://doi.org/10.1007/bf00674341) (cited on page 2).
- [6] H. Iams and B. Salzberg. "The Secondary Emission Phototube". In: *Proceedings of the IRE* 23.1 (1935), pp. 55–64. doi: [10.1109/jrproc.1935.227243](https://doi.org/10.1109/jrproc.1935.227243) (cited on page 2).
- [7] T. Bednarski et al. "Calibration of photomultipliers gain used in the J-PET detector". In: *Bio-Algorithms and Med-Systems* 10.1 (2014), pp. 13–17. doi: [10.1515/bams-2013-0110](https://doi.org/10.1515/bams-2013-0110) (cited on page 2).
- [8] A. Einstein. "Über einen die Erzeugung und Verwandlung des Lichtes betreffenden heuristischen Gesichtspunkt". In: *Annalen der Physik* 322.6 (1905), pp. 132–148. doi: [10.1002/andp.19053220607](https://doi.org/10.1002/andp.19053220607) (cited on page 2).
- [9] A. G. Wright. *The Photomultiplier Handbook*. Oxford University Press, 2017, p. 624 (cited on page 3).
- [10] IceCube Collaboration, R. Abbasi et al. "Calibration and characterization of the IceCube photomultiplier tube". In: *Nuclear Instruments and Methods in Physics Research Section A: Accelerators, Spectrometers, Detectors and Associated Equipment* 618.1-3 (2010), pp. 139–152. doi: [10.1016/j.nima.2010.03.102](https://doi.org/10.1016/j.nima.2010.03.102) (cited on page 3).
- [11] Icecube Collaboration, M. Aartsen et al. "The IceCube Neutrino Observatory: instrumentation and online systems". In: *Journal of Instrumentation* 12.03 (2017), P03012–P03012. doi: [10.1088/1748-0221/12/03/p03012](https://doi.org/10.1088/1748-0221/12/03/p03012) (cited on pages 3, 4).
- [12] M. Ahlers, K. Helbing, and C. P. de los Heros. "Probing particle physics with IceCube". In: *The European Physical Journal C* 78.11 (2018). doi: [10.1140/epjc/s10052-018-6369-9](https://doi.org/10.1140/epjc/s10052-018-6369-9) (cited on page 4).
- [13] T. Benson et al. "IceCube Enhanced Hot Water Drill functional description". In: *Annals of Glaciology* 55.68 (2014), pp. 105–114. doi: [10.3189/2014aog68a032](https://doi.org/10.3189/2014aog68a032) (cited on page 4).

